Proceedings of the 12th International Conference on
Alkali-Aggregate Reaction in Concrete

LATE-EXPANSIVE ALKALI-SILICA REACTION IN THE OHNYU AND FURIKUSA HEADWORK STRUCTURES, CENTRAL JAPAN

Tetsuya Katayama[a) *], Yoshinori Sarai[a)], Yoshimi Higashi [b)] and Akihiko Honma [b)]
a) Kawasaki Geological Engineering Co. Ltd., 2-11-15 Mita, Minato-ku,Tokyo, 108-8337 Japan
b) Japan Water Agency, 26 Ohshima, Kawai, Hohrai-cho, Minamishitara, Aichi, 441-1601 Japan

ABSTRACT

Detailed petrographic diagnosis was done on the two headwork structures with a small dam/canal complex, to identify the mechanisms of their deterioration. It was confirmed that the deterioration was due to late-expansive ASR of sandstone, mudstone, metamorphic hornfels and gneiss in the gravel aggregate used, and that the original cement used contained at least 0.82-0.84% of Na_2Oeq. Highly damaged concrete produced smaller expansion in the accelerated core expansion test, suggestive of a smaller potential for residual expansion. The origin of abundant ettringite was a result of severe cracking due to ASR, and not the sulfate attack due to the pyrite contained.

Keywords: Alkali-silica reaction, ASR gel, EPMA analysis, ettringite formation, sulfate attack

1 INTRODUCTION

The Toyogawa Canal System of central Japan contains several hydraulic structures for agricultural purposes. Among these, two concrete structures have been deteriorating. At Furikusa headwork, the span of two weir pillars supporting the spillway gate has been narrowed (4cm/6m) from the construction time, and frequent mechanical maintenance has been made to mitigate the distortion. Ohnyu headwork, located 10 km northwards, has similar deterioration. These structures (construction: 1968) exhibit extensive map-cracking, and early investigations in 1995-1996 [1, 2] reported that the causative factors for deterioration were alkali-aggregate reaction and sulfate attack.

The crack width of these structures has been growing in the past few years (Table 1). It was therefore decided to clarify the nature and the extent of the damage, based on detailed petrographic examinations of core samples, in order to provide fundamental data for planning a long-term rehabilitation program [3].

Wide vertical cracks (width 10 mm) developed on the crest of some structurural members where water is accessible and reinforcing bars were sparse. Even with these cracks, reinforcing bars were not particularly stained, which was confirmed by the half-cell potentials of the bars and visual inspection of them through boreholes. Carbonation depth was less than 1cm, owing to the wet condition of structures rich in hyfroxyl ions (abundant portlandite).

Table 1 Site of major core sampling at two headwork structures (diameter 10 cm, length 25-50 cm)

Structure	Ohnyu			Furikusa		
Site	1	2 x)	5 x)	1 x)	2	5 x)
Concrete member	Spillway Wall crest Pillar #2	Pillar #3 Terrace	Pillar #3 Wall	Pillar #3 Terrace	Fish ladder Wall crest	Pillar #3 Wall
Access to water	Rain, river	Rain, river		Rain, river	Rain, river	
Coring direction	Vertical	Vertical	Horizontal	Vertical	Vertical	Horizontal
Vertical cracking	Severe	Severe	None	Severe	Severe	None
Width (max)	10 mm	3 mm		10 mm	10 mm	
Growth (width /8 years)	4.8 mm	2.6 mm		5.0 mm	8.8 mm	
Depth (max)	205 mm	321mm		330 mm	382 mm	

x) Small cores (diameter 5 cm, length 13 cm) were also taken for accelerated expansion test

*) e-mail: Katayamat@kge.co.jp

2 PETROGRAPHIC EXAMINATION

2.1 Core scanning

Concrete cores (diameter 10cm, length 50cm) were subjected to core scanning to reveal the mode of crack propagation inside the concrete, as well as the maximum depth of cracking. The result of the measurements of vertical cracks are given in Table 1.

Fig.1 shows that the crack pattern was controlled by the strain distribution in concrete, i.e. a wide vertical crack (10 mm across, two sectors in the figure) was opened to the surface of concrete, extending from narrow and horizontally oriented cracks inside the concrete. This is a result of liberation of the expansion force generated by alkali-silica reaction (ASR), which had been constrained by the reinforcing bars (depth 8-12cm) that rim the structure.

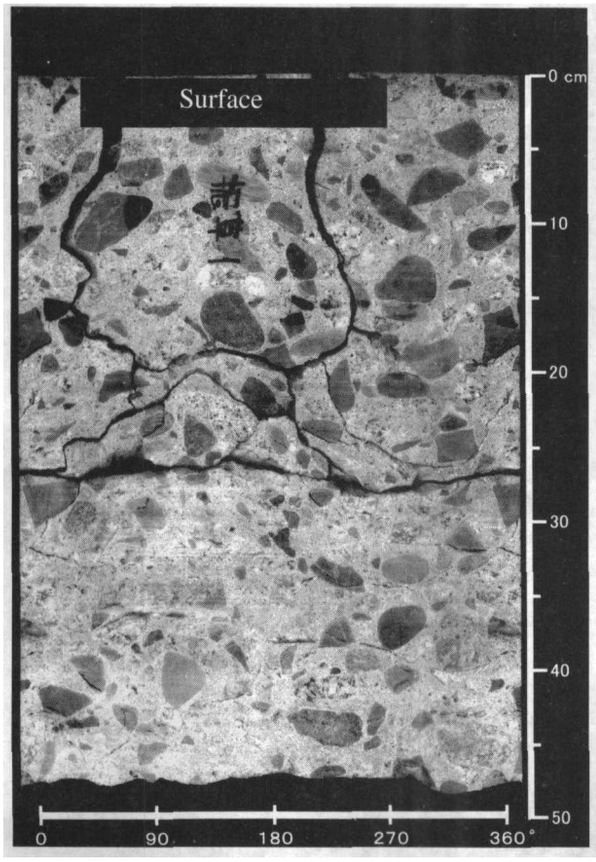

Fig.1 Core scanning of a severely cracked concrete (Furikusa-1)

2.2 Macroscopic examination

While reaction products of ASR were not evident on the core surface (Fig. 1), they were strikingly pronounced on the fracture surface of the concrete. Fig. 2 is a close-up view of a white reaction rim, formed on the coarse aggregate particles of gneiss and mudstone, along with white deposits that had exuded into the cement paste along the cracked plane, now exposed by fracturing.

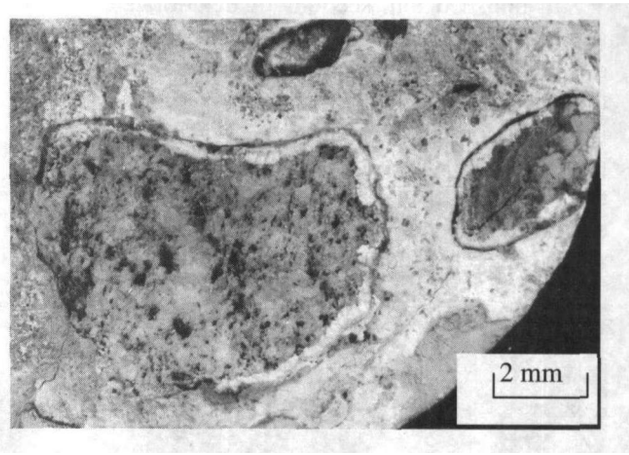

Fig.2 Fracture surface of concrete showing reacted gneiss (Furikusa-1)

Beside ASR gel, cracks and air-voids in concrete were often filled with white deposits of ettringite.

2.3 Point counting

Coarse aggregate in the Ohnyu and Furikusa concretes was gravel with a similar lithology. Almost all sedimentary rocks contained (sandstone, mudstone, siliceous shale and chert) and some particles of metamorphic rocks (hornfels, biotite schist and gneiss) have been undergoing ASR (Table 2). They all are late-expansive ASR rock types, containing crypto- to microcrystalline quartz, and the reaction of schist and gneiss is the first reported occurrence in Japan.

Table 2 Lithology of coarse aggregate in concrete

Rock type	Ohnyu			Furikusa		
	1	2	5	1	2	5
Sandstone [1)]	24.0	12.3	13.0	29.0	30.8	28.6
Mudstone [1)]	9.3	3.3	10.4	11.7	7.7	4.9
Siliceous shale [1)]		0.8	2.6	7.5	3.5	6.4
Chert [1)]	9.1	8.0	4.1	7.4	6.2	1.0
Welded tuff	1.0	0.8	1.6	2.2	2.1	3.0
Tuff	0.1			0.2		
Porphyrite	1.7	1.6				
Meta-diorite		2.0				
Amphibolite	7.3	2.9	2.1	2.2	0.5	6.4
Hornfels [2) 3)]	5.1	1.5	8.8	3.0	6.3	6.9
Biotite schist [2)]	2.0	1.9	2.6	1.4	3.0	3.9
Quartz schist	2.6	0.8	4.0	1.1	1.6	1.0
Gneiss [2)]	21.6	34.5	28.0	13.3	14.5	18.7
Granite	16.2	29.6	22.8	21.0	23.8	19.2

[1)] All particles exibit ASR on fracture surface
[2)] Some particles exibit ASR on fracture surface
[3)] Possibly underestimated due to vidual counting

2.4 Polarizing microscopy

In polished thin sections of deteriorated Ohnyu and Furikusa headwork concretes, three major types of ASR gel were recognized: 1) crack-filling gel in the reacted aggregate, representing the initial stage of gel formation, 2) crack-filling ASR gel in the cement paste, characterizing the migration stage of the gel, and 3) air void-filling gel, usually typical of the late stage (where the air void contacts the reacted aggregate, gel in the voids has the nature of a gel 1)).

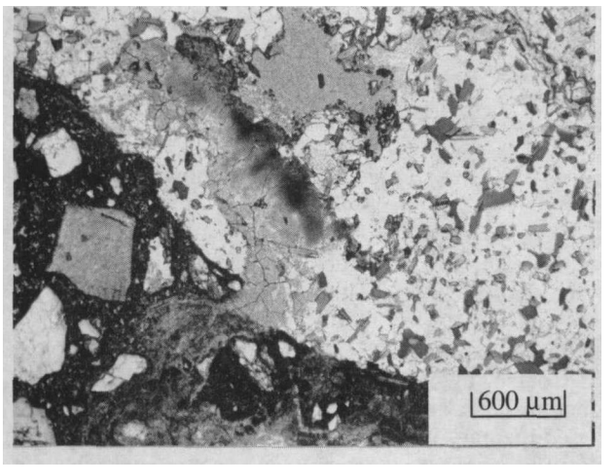

Fig 3 Reacted hornfels exuding ASR gel (Ohnyu-1)

2.5 SEM observation

Following the polarizing microscopy, polished thin sections were subjected to SEM observation as a preliminary step in element mapping and quantitative EPMA (EDS) analysis to check the chemical compositions of ASR gel, CSH gel and unhydrated cement clinker phases in the cement paste.

Amorphous ASR gel rich in alkalies, exhibits pronounced evidence of volume change during wetting and drying (expansion and drying shrinkage). With time this type of gel crystallizes into lamellar balls or, typically, rosette-like aggregates composed of minute flaky crystals. Figs.4 and 6 show examples filling cracks within reacted sandstone coarse aggregate. It is noteworthy that the chemical compositions of both amorphous and crystallized gel (rosette) are essentially the same, as shown in Table 3.

It is reasonable to assume that the rosette-like crystalline phase is no longer expansive, since it is not a gel. However, the coexistence of amorphous ASR gel rich in alkalies suggests that this gel will display a great volume change when it becomes wet, and expansion of concrete will still continue.

On the other hand, abundant occurrence of the rosette-like phase in the concrete would indicate that ASR had occurred intensively in the past, which explains the higher magnitude of the concrete deterioration observed at present.

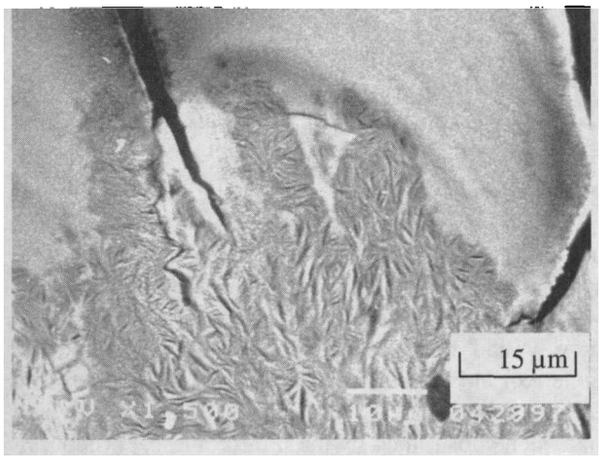

Fig.4 SEM photograph of partly crystallized ASR gel, filling a crack of sandstone aggregate (Ohnyu-2)

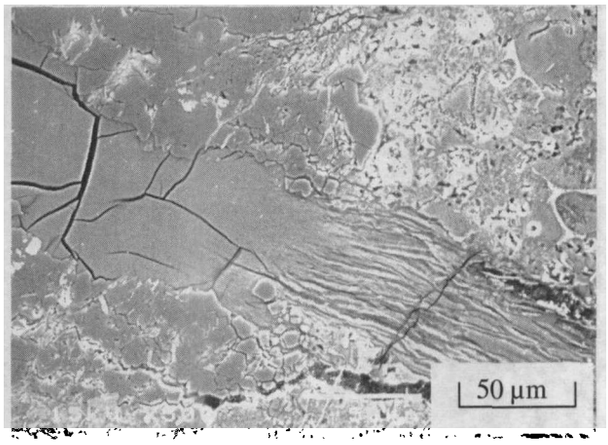

Fig.5 SEM photograph of ASR gel exuding from sandstone aggregate into cement paste (Furikusa-2)

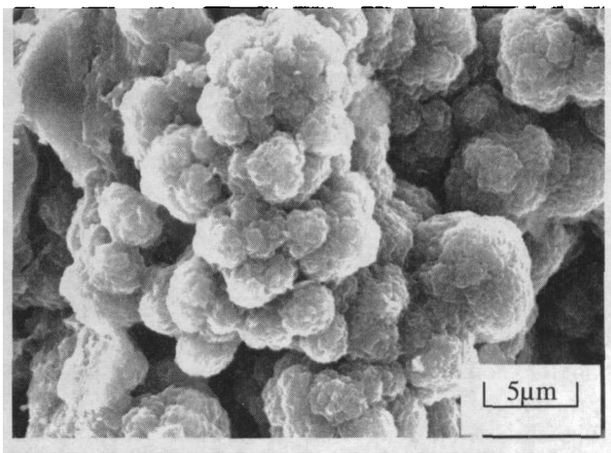

Fig 6 ASR gel crystallized into lamellar balls, resembling aggregate of gyrolite (Ohnyu-2)

2.6 EPMA analysis of ASR and CSH gel

Compositional changes of both ASR gel and CSH gel in concrete (depth 30-40 cm) have been determined by EPMA (EDS), as shown in Fig.7. Three deteriorated concretes (Ohnyu-1, 2, Furikusa-2) had similar reaction trends, and generally resemble the trends obtained from Newfoundland concretes [4]. However, the position of a convergent point between the three trend lines (hydration of alite, belite and evolution of ASR gel) was more calcium-rich in the Ohnyu and Furikusa concretes, i.e. the effect of weathering, freezing and thawing, and leaching was less marked than in Newfoundland.

In Fig.7, crack-filling ASR gel in the reacted aggregate has the lowest [Ca/Si] and [Ca/(Na+K)] atomic ratios (lower left). The gel gains calcium and loses alkalies during migration along cracks in the cement paste, approaching compositions of CSH gel. Both CSH gel and ASR gel in the concretes probably exist in equilibrium with portlandite at around [Ca/Si] = 1.5, since concretes with this depth were fresh and rich in portlandite crystals.

On the left side of the Fig.7, the compositional line of ASR gel passes a ppoint at [Ca/Si] = 1/3, [Ca/(Na + K)] = 1.0, where rosette-like crack-filling ASR gel is expected. This point corresponds to 2CaO $(Na, K)_2O$ $6SiO_2$ nH_2O, and, if alkalies $(Na, K)_2O$ are replaced by 2CaO, then it resembles gyrolite 2CaO $3SiO_2$ $2H_2O$. This mineral has a similar habit to present lamellar-ball or rosette-like aggregations. This line also passes a point of [Ca/Si] = 1/6, [Ca/(Na + K)] = 1/2, similarly corresponding to CaO $(Na, K)_2O$ $6SiO_2$ nH_2O, or okenite CaO $2SiO_2$ $2H_2O$.

Table 3 Chemical compositions of amorphous and crystallized ASR gel filling cracks of aggregate

	Ohnyu				Furikusa	
	1		2		2	
	Mudstone		Sandstone		Sandstone	
	Vein	Vein	Vein	Vein	Vein	Vein
	Amor-phous	Rose-tte	Amor-phous	Rose-tte	Rose-tte	Rose-tte
SiO_2	41.37	37.22	40.71	41.60	47.56	40.85
TiO_2	0.00	0.26	0.00	0.24	0.00	0.34
Al_2O_3	0.11	0.50	0.04	0.00	0.15	0.03
Fe_2O_3	0.00	0.11	0.68	1.05	0.00	0.35
MgO	0.00	0.00	0.00	0.00	0.00	0.00
CaO	11.47	9.36	11.51	10.28	7.52	9.85
Na_2O	4.12	2.39	6.11	3.54	3.24	3.53
K_2O	6.61	8.55	6.28	8.15	7.48	8.63
SO_3	0.19	0.10	0.32	0.00	0.31	0.34
P_2O_5	0.19	0.00	0.00	0.22	0.00	0.00
Total	64.19	58.49	65.65	65.08	66.26	63.92
[Ca/Si]	0.30	0.27	0.30	0.26	0.17	0.26
[Ca/Na+K]	0.75	0.65	0.62	0.64	0.51	0.59

However, because okenite is needle-shaped, different from common ASR products, further study is needed to identify a related phase in concrete.

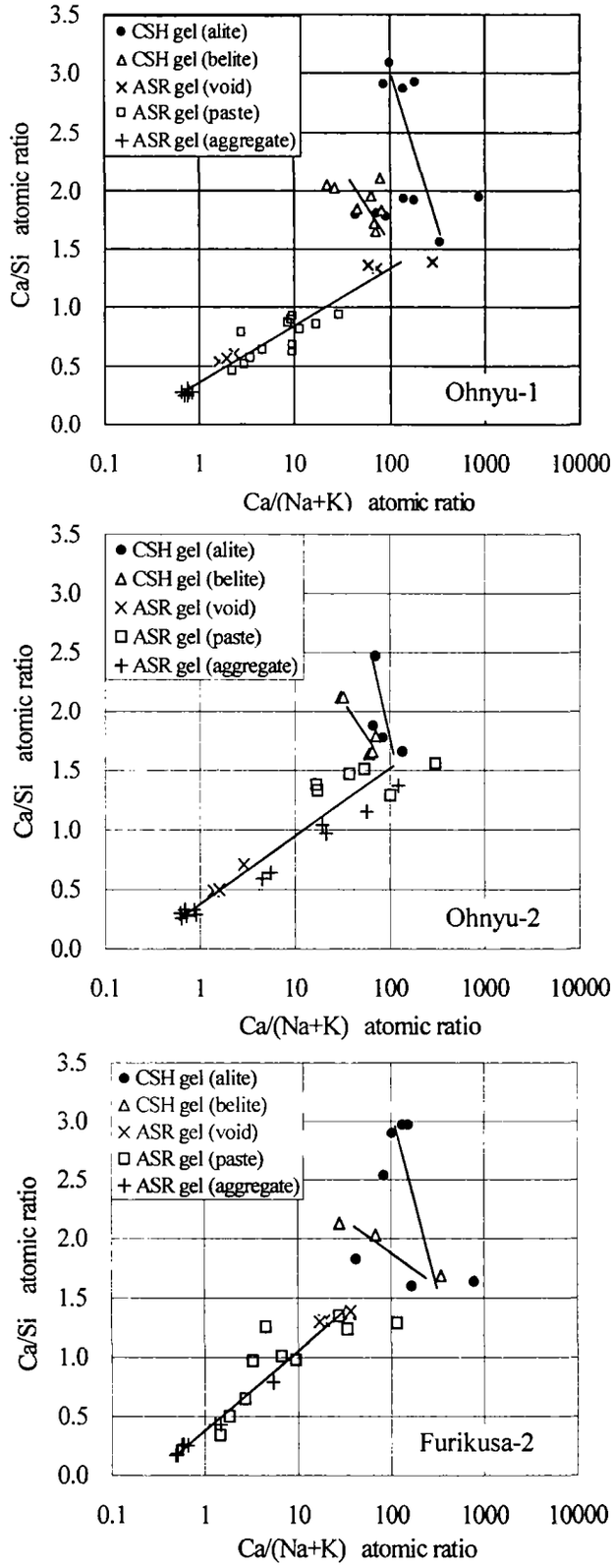

Fig.7 Compositional changes of ASR gel and CSH gel in deteriorated concretes as determined by EPMA

2.7 Estimation of minimum cement alkali

Polarizing microscopy of polished thin sections (depth at 30-40 cm) revealed that Portland cement used in the Ohnyu and Furikusa headwork structures had been well-hydrated, leaving pseudomorphic textures composed of transparent CSH gel after alite and belite, and of dark hydrated interstitial phases after calcium aluminate and ferrite. Abundant crystals of portlandite in cement paste surround these cement particles.

The original size of cement grains, as evaluated through the image of hydrated pseudomorphs, was moderately fine, and not particularly different from that of modern Portland cement. The size of calcium silicates (alite and belite) was generally small, and associated interstitial phases (aluminate and ferrite) were also fine-grained and uniformely oxidized. These suggest that the original cement clinker was relatively in small nodules, and that it was burnt in a rapidly, followed by efficient cooling, suggesting production by the Lepol kiln.

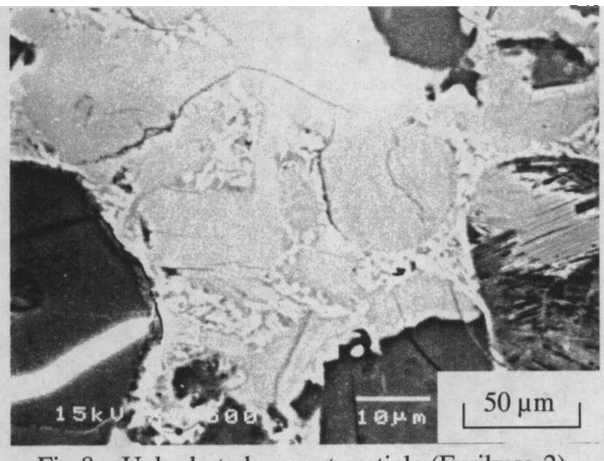

Fig.8 Unhydrated cement particle (Furikusa-2)

Since there was no record about the chemical composition of the cement used, it was decided to estimate the alkali content of the original cement, based on EPMA analysis of unhydrated cement clinker phases after Katayama [5]. However, as described earlier, cement hydration had proceeded in these hydraulic structures, and it was generally difficult to find unhydrated cement particles whose sections appeared on the plane of the polished thin section, even though polarizng microscopy detected the presence of unhydrated grains in the thickness (15-20 μm) of the specimen.

It was revealed that the concretes from the two structures (Ohnyu-1, Furikusa-2) contained high-alkali cement with at least 0.82 to 0.84 % of Na_2Oeq. The original level of the cement alkali would have been higher, possibly up to 30%, since water-soluble alkali sulfates were not preserved in concrete and hence not evaluated. Titanium was characteristically contained in the cement clinker used, reflecting the local nature of the raw materials used.

Considering that the headwork structures are subjected to a moist environment, ASR can be promoted with this level of cement alkali, even though a late-expansive type of aggregate (including very slow reactive biotite schist and gneiss) was used. Simillar situations exhist in many hydroelectric dams in the continental regions throughout the world. Durand et al [6] reported a similar case of a Canadian dam, in which late-expansive ASR due to biotite schist had been resulted from the cement containing at least 0.8-1.0 % of Na_2Oeq, and the possibility of sulfate attack was investigated as well.

Table 4 Unhydrated cement and estimated minimum alkali content of original cement based on EPMA analysis

	Ohnyu-1				Furikusa-2			
	Alite	Belite	Aluminate	Ferrite	Alite	Belite	Aluminate	Ferrite
SiO_2	25.06	31.14	5.09	5.73	24.99	31.11	5.17	4.39
TiO_2	0.39	0.60	0.93	1.24	1.02	0.86	1.02	1.82
Al_2O_3	0.57	1.86	24.45	19.87	1.07	1.42	26.79	21.61
Fe_2O_3	0.96	0.92	11.68	19.51	0.65	1.26	7.68	20.36
MgO	1.11	0.73	2.24	4.25	0.54	0.29	1.34	3.70
CaO	69.09	60.02	49.28	43.19	68.66	59.67	50.72	44.92
Na_2O	0.22	0.48	2.70	0.49	0.22	0.76	2.73	0.32
K_2O	0.21	0.88	1.02	0.42	0.14	0.58	1.22	0.42
SO_3	0.00	0.07	0.21	0.09	0.02	0.09	0.08	0.35
P_2O_5	0.15	0.00	0.00	0.09	0.07	0.24	0.00	0.30
Total	97.76	96.70	97.60	96.88	97.38	96.28	96.76	98.19
Na_2O_{eq}*)	0.22	0.21	0.34	0.08	0.19	0.23	0.35	0.05
Total Na_2O_{eq}	0.85				0.82			

*) Assumption: Alite 60%, belite 20%, aluminate 10%, ferrite 10%

2.8 Examination of sulfate attack

Early study of these headwork structures in 1995 [1] suggested that ASR had already ceased by that time, because the conventional JCI concrete core expansion test only produced small expansion (< 0.02% at 6 months). Instead, it was emphasized that sulfate attack due to the formation of ettringite derived from iron sulfide in the aggregate, would produce continuing expansion of concrete.

Subsequent study in 1996 [2] indicated that coarse aggregate used contained 0.01 to 0.05% of sulfide sulfur (S), corresponding 0.02 to 0.09% of pyrite, and assumed that even such a small amount of sulfur could cause expansion, as a result of delayed ettringite formation through the bacterial action to be expected in the wet environment of the structures.

However, no observation has been made in the previous studies confirming that ettringite was actually being formed around or from the pyrite in the aggregate. Consequently, this paper conducts detailed petrographic examination of the interfacial zone between pyrite grains exposed to the aggregate surface and the surrounding cement paste (Table 5).

2.9 The occurrence of pyrite

In both Ohnyu and Frikusa concretes, pyrite occurs sporadically in the sandstone coarse aggregate as blastic grains or framboidal aggregations of minute grains (Fig.9). In much sandstone gravel, pyrite had been altered to a pseudomorphic texture composed of hematite and limonite leaving a rust-stain. Since weathered sandstone gravel is also visible in the deeper portions of concrete, where secondary oxidation was unlikely to occur, this alteration is attributable to the geological weathering, and not a secondary reaction that might be expected to occur after the use of aggregate into concrete.

Pyrite is also present as idiomorphic cubes in hornfels of lower metamorphic grade (Fig.11), or in sandstone. Framboidal pyrite is more susceptible to weathering due to its larger specific surface area (smaller size) than idiomorphic pyrite. This may occur in the outcrops or in gravel quarries.

Table 5 Hydrates in the contact zone between pyrite and cement paste

Pyrite	Ohnyu		Furikusa	
	1	2	1	2
Sandstone				
Framboidal	CSH/Ett*)			Ettringite
Idiomorphic		CSH		
Hornfels				
Idiomorphic			CSH/Ett*)	

*) Ett: Ettringite

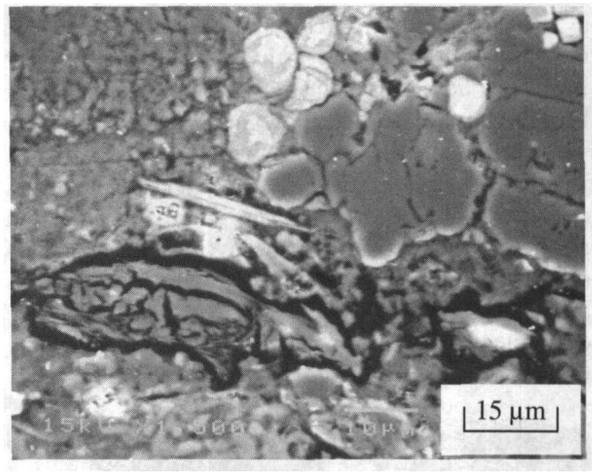

Fig.9 Framboidal pyrite contacting CSH gel and crack-filling ettringite (Ohnyu-1)

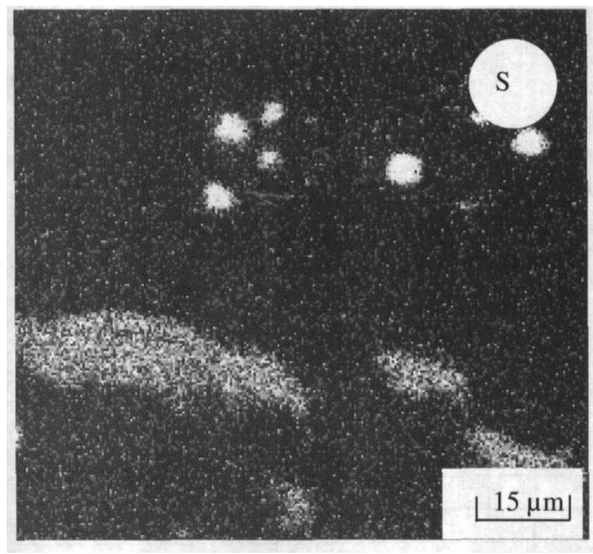

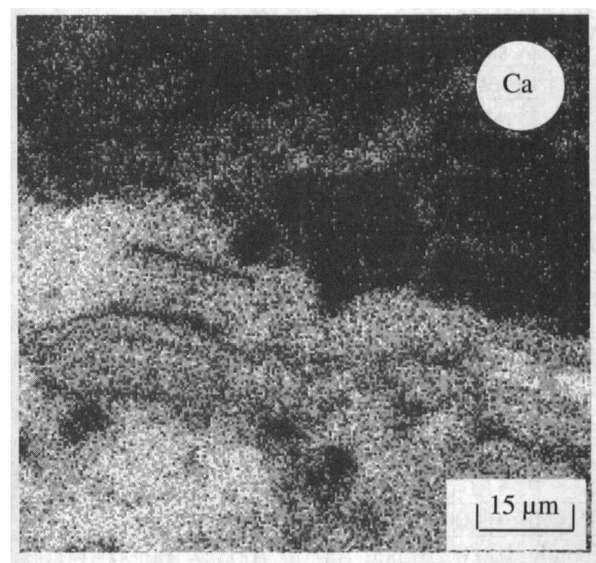

Fig 10 Distribution of sulfur and calcium at the interface between pyrite and cement paste (Fig.9)

2.10 Mapping of elements around pyrite

Detailed EPMA (EDS) analysis of the interface between pyrite and cement paste was done to show the distribution of elements (Table 6, Figs10,12). Fresh pyrite FeS_2 in the aggregate has a stoichiomety with [S/Fe] atomic ratio of 2.0 (1.97), while weathered pyrite selectively lost sulfur and decreases down to 1.2. Its end products were hematite and limonite. CSH gel around the pyrite grains took up small amounts of SO_3 and Fe_2O_3, but their level was too low (SO_3 <1%, Fe_2O_3 <5%) to form secondary ettringite. This suggests that pyrite did not contribute to the formation of secondary ettringite in concrete.

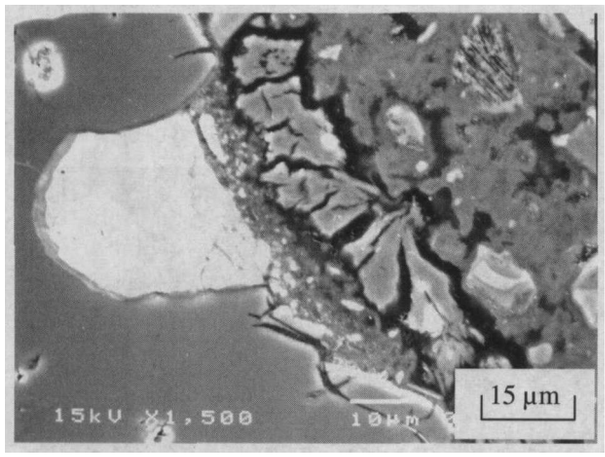

Fig 11 Idiomorphic pyrite contacting cement paste (CSH gel) and crack-filling ettringite (Furikusa-1)

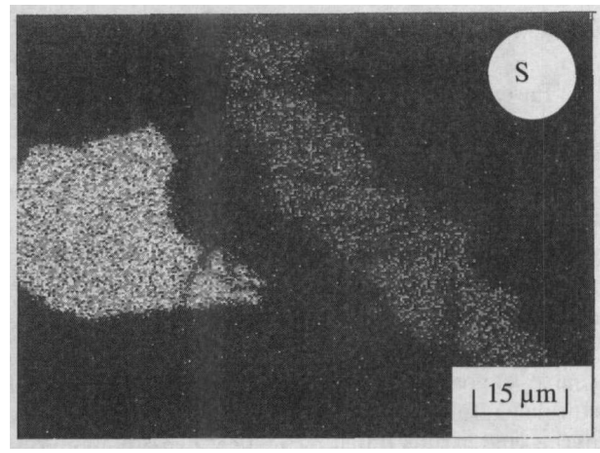

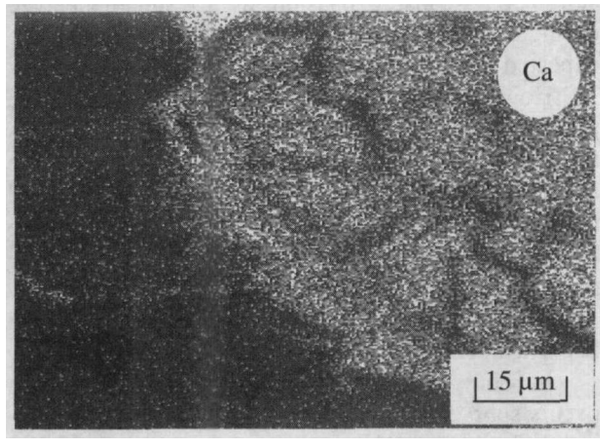

Fig 12 Distribution of sulfur and calcium at the interface between pyrite and cement paste (Fig. 11)

Table 6 Composition of pyrite and surrounding cement hydrates

Pyrite							Weathered products of pyrite and cement hydrates						
	Ohnyu			Furikusa				Ohnyu				Furikusa	
	1	2		1	2			1			2	1	
	Sand-stone	Sandstone		Horn-fels	Sandstone			Limonite	Hematite	CSH gel	CSH gel	CSH gel	Port-landite
	Fresh	Fresh	Altered	Altered	Fresh	Altered		Altered	Altered	near	near	near	near
	Fram-boidal Core	Idio-morphic	Idio-morphic	Idio-morphic	Idio-morphic	Fram-boidal		Fram-boidal Rim	Blastic	Fram-boidal	Idio-morphic	Idio-morphic	Idio-morphic
Si	1.62	1.62	1.52	1.43	1.66	1.47	SiO_2	11.99	3.30	19.88	20.66	18.59	1.03
Ti	0.00	0.25	0.61	0.00	0.02	0.39	TiO_2	0.00	0.47	0.54	0.05	0.29	0.00
Al	0.01	0.21	0.15	0.00	0.11	0.05	Al_2O_3	2.33	1.41	3.58	2.07	3.96	0.26
Fe	46.60	45.63	54.79	57.00	46.00	56.84	Fe_2O_3	57.52	90.01	3.82	1.04	4.58	0.54
Mg	0.14	0.13	0.00	0.44	0.01	0.19	MgO	0.00	0.00	0.00	0.00	0.43	0.00
Ca	0.15	0.12	0.40	0.00	0.27	0.27	CaO	11.94	0.28	34.63	30.75	27.22	69.42
Na	0.06	0.38	0.52	0.03	0.00	0.36	Na_2O	0.92	1.18	0.21	0.61	0.35	0.20
K	0.39	0.00	0.00	0.01	0.00	0.00	K_2O	0.40	0.51	0.45	0.00	0.18	0.18
S	51.04	51.65	42.02	41.09	51.94	40.40.	SO_3	1.26	0.18	0.69	0.63	1.01	0.13
P	0.00	0.00	0.00	0.00	0.00	0.00	P_2O_5	1.75	0.24	0.00	0.27	0.00	0.00
Total	100.0	100.00	100.00	100.00	100.00	100.00	Total	88.21	97.58	63.81	56.11	56.86	71.78
[Fe]*)	1.00	1.00	1.00	1.00	1.00	1.00	[Ca/Si]			1.87	1.59	1.57	
[S] *)	1.91	1.97	1.34	1.26	1.97	1.24							

*) Atomic ratio, normalized to Fe =1.00

2.11 Ettringite formation in concrete

Ettringite occurs filling cracks and interstices between the aggregate and cement paste (Fig.13), as well as in air voids. Detailed SEM observations, coupled with element mapping and quantitative EPMA (EDS) analysis of the polished thin sections (mainly x 1000-2000, 0.05nA), revealed that both pyrite and its weathered products on the aggregate surface were mostly covered with CSH gel in the cement paste, and that cracks opened adjacent to the cement-aggregate interface were filled with ettringite veins (Figs.9,11). Portlandite was intimately associated with this ettringite (Fig.11, upper margin).

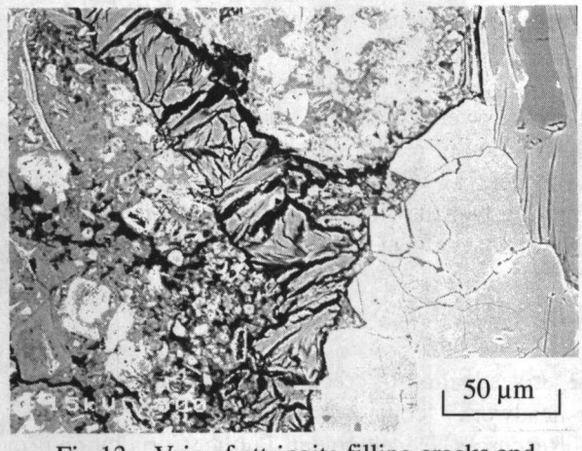

Fig 13 Vein of ettringite filling cracks and interstices in concrete (Furikusa-2)

These suggest that 1) the aggregate and cement paste was originally well-bonded, and that 2) cracks were opened later near the aggregate surface, along which ettringite and portlandite had precipitated. This means that pyrite has nothing to do with the delayed formation of ettringite, and that cracking in concrete was caused by expansion due to ASR In other words, sulphate attack did not take place, and the formation of ettringite veins was not the cause of deterioration, but resulted from cracking due to ASR Such secondary ettringite has been noted in severely cracked concrete undergoing ASR.

Chemical compositions of ettringite are shown in Table 7. The total analysis of the stoichiometric ettringite $3CaO\ Al_2O_3\ 3CaSO_4\ 32H_2O$ should be 54.1%, but the result was around 65%, like that of monosulfate. This is due to dehydration of some molecules under the evacuating procedures and the effect of heating by the electron beam, which took place during the storage of thin sections, carbon coating and EPMA analysis. To minimize the differences in results, where possible, crystal bundles cut vertical to their C-axes were chosen for analysis.

There was little difference among compositions of ettringite, whether it was in contact with pyrite or not. The results conform with the stoichiometry of ettringite, with some impurities taken in the solid solution of $Ca_6\ (Al, Fe)_2\ (S, Si)_3O_{18}\ nH_2O$, but no evidence has been noted that a thaumasite component was present. Crystals cut in the elongated direction gave a poor stoichiometry.

Table 7 Compositions of ettringite in the deteriorated concrete

	Ohnyu					Furikusa				
	1			2		1		2		
	Crack		Void	Crack	Void	Crack		Crack		Void
	Facing framboidal pyrite	Facing aggregate	Radial bundles	Facing aggregate	Radial bundles	Facing idiomorphic pyrite	Cement paste	Facing framboidal pyrite	Cement paste	Radial bundles
SiO_2	0.29	0.38	0.17	0.03	0.22	0.03	0.25	22.45	0.23	0.23
TiO_2	0.01	0.23	0.07	0.45	0.37	0.00	0.00	0.12	0.00	0.26
Al_2O_3	9.38	9.72	9.47	9.78	9.91	10.29	9.97	9.74	9.10	9.64
Fe_2O_3	0.50	0.04	0.00	0.16	0.00	0.03	0.58	0.54	0.00	0.00
MgO	0.00	0.00	0.00	0.00	0.00	0.00	0.00	0.00	0.00	0.00
CaO	30.35	31.56	31.92	32.78	32.47	32.24	34.39	33.40	32.72	33.30
Na_2O	0.00	0.13	0.00	0.04	0.19	0.20	0.15	0.13	0.07	0.04
K_2O	0.12	0.28	0.00	0.00	0.00	0.01	0.30	0.22	0.00	0.17
SO_3	22.61	22.25	22.93	22.34	23.29	23.22	23.14	22.45	23.12	23.63
P_2O_5	0.25	0.00	0.17	0.09	0.23	0.50	0.42	0.30	0.09	0.00
Total	63.52	64.60	64.71	65.66	66.68	66.52	69.21	67.52	65.35	67.27
[Ca]*)	5.76	5.94	5.95	6.09	5.89	5.85	6.08	6.05	6.07	6.01
[Al]*)	1.96	2.01	1.95	2.00	1.98	2.05	1.94	1.94	1.86	1.91
[Fe]*)	0.07			0.05			0.07	0.07		
[Si]*)	0.05	0.07	0.03	0.01	0.06		0.04	0.11	0.04	0.04
[S]*)	3.00	2.94	2.99	2.91	2.96	2.95	2.86	2.85	3.01	2.99

*) Normalized to O =18: $Ca_6\ (Al, Fe)_2\ (S, Si)_3O_{18}\ nH_2O$

3 ACCELERATED EXPANSION TEST

An accelerated concrete core expansion test (80°C 1M NaOH, diameter 5cm, length 13 cm) was performed (Fig.14). All the core samples produced relatively small but linear expansions even at 3 months, suggestive of a late-expansive nature of ASR.

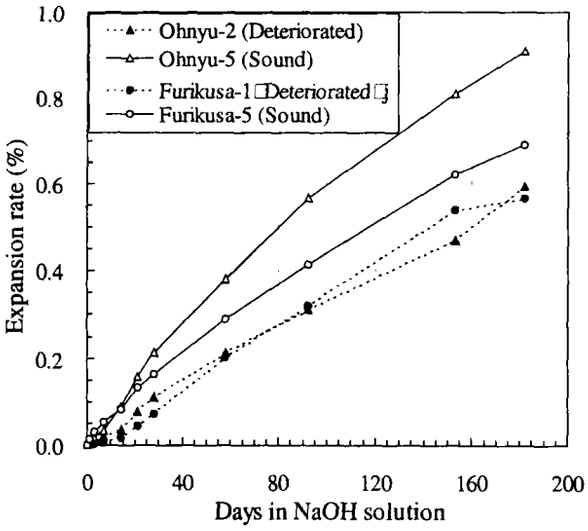

Fig.14 Expansion of accelerated concrete core test

Expansion of core samples from the sound portions (Ohnyu-5, Furikusa-5) exceeded 0.10% at 21 days, a preliminary limit for gravel aggregate containing highly reactive andesite in Japan [7]. It is remarkable that cores from the deteriorated portions of two headwork structures (Ohnyu-2, Furikusa-1) presented smaller expansions while they contain the same aggregate (Table 2).

This suggests that reactive minerals in the deteriorated concretes had been consumed more during the process of field ASR, and that there are relatively smaller proportions left for further reaction. On the other hand, concrete in the sound portions still contains larger amount of reactive minerals, and hence has a higher potential for producing residual expansion in the field concrete, if conditions were met to accelerate ASR.

It is reasonable to lower the expansion limit for the late-expansive ASR in the accelerated concrete core expansion test.

4 CONCLUDING REMARKS

(1) Both Ohnyu and Furikusa headwork concretes are undergoing late-expansive ASR, due to sedimentary (sandstone, mudstone and chert) and metamorphic rocks (very slow-reactive schist and gneiss) contained in the gravel aggregate used.

(2) Deleterious alkali-rich ASR gel has been partly crystallized into an inert phase (rosettes) in old cracks within reacted aggregate particles, but where this amorphous gel is present, it is assumed swelling (expansion) of concrete will continue. An accelerated concrete core expansion test can also be used for evaluating the potential for future reaction of concrete.

(3) There was no evidence that sulfate attack and intense sulfate migration had occurred around the pyrite grains in the aggregate. Abundant ettringite, filling cracks and air voids in concrete, was the result of ASR which had cracked concrete and facilitated dissolution of the cement paste and precipitation of secondary ettringite along these cracks, and was not the cause of the deterioration.

(4) Wide cracks opening in some places in the concrete were probably the result of 1) sparse distribution of reinforcing bars, 2) permanent supply of water, 3) combined effect of ASR and local freezing and thawing, and 4) high alkali content of the original cement used (Na_2Oeq 0.82-0.84).

REFERENCES

[1] Investigation of cracking in Furikusa and Ohnyu headwork concretes, August, 1995, Water Resources Development Public Corporation. (in Japanese)

[2] Investigation on the state of headwater facility, November, 1996, Water Resources Develop-ment Public Corporation (in Japanese)

[3] Diagnosis of headwater concrete facility, March, 2003, Water Resources Development Public Corporation (in Japanese)

[4] Katayama T., Bragg D.J., Alkali-aggregate reaction combined with freeze/thaw in Newfound-land, Canada - Petrography using EPMA, Proc. 10th ICAAR, Melbourne, Australia, 243-250

[5] Katayama T, Petrographic diagnosis of alkali-aggregate reaction in concrete based on quantitative EPMA analysis, Proc. 4th CANMET /ACI/JCI Int.Conf.Recent Advances in Concrete Technology, Tokushima, Japan, 539-560

[6] Durand B, Marchand B, Larivere, R, Bergeron, J=M, Pelletier, G, Ouimet, M, Berard, J, Katayama, T, A special history case about severe damages due to freezing and thawing combined with sulfate migration and ASR at Rapides-des-Quinze hydraulic structures, Quebec, Canada, Proc. 12th ICAAR, Beijing, China

[7] Katayama T, Tagami M, Sarai, Y, Izumi S, Hira T, Alkali-aggregate reaction under the influence of deicing salts in the Hokuriku district, Japan, Proc.9th Euroseminar on Microscopy Applied to Building Materials, Trondheim, Norway